ratios, the C/I ratio was varied, and subjective viewing of the resulting demodulated video signal was used to determine the "perceptibility threshold", at which the effects of the interference could barely be discerned. This threshold was determined for different offset frequencies, for which the relative frequency between the center of the interferer and the center of the video signal. The results of these tests are several interference perceptibility threshold curves. These curves provide information on the minimum C/I which must be maintained in the LMDS/FSS systems to avoid a perceptible effect on the quality of the video signals.

The second set of tests made use of NASA Lewis's INTEX Ka-band experiment ground terminal to allow field measurements of the amounts of interferer power received by some typical Ka-band antennas. NASA currently operates the only Ka-band satellite system in the Western Hemisphere; the INTEX terminal is a 2.44 meter aperture ground terminal, designed for low to high data rate experiments with the ACTS. Several members of the IWG, including both the LMDS and satellite industries, were interested in field tests since the propagation and reflection characteristics of 28 GHz signals are not well documented.

The NASA Lewis field tests consisted of operating the INTEX terminal in a normal manner, consisting of transmitting a CW tone while pointed to the ACTS satellite. The elevation angle from the Cleveland, Ohio, location of INTEX to the ACTS satellite, located at 100° West longitude, is 38°. The INTEX terminal was operated near it's maximum transmit power, resulting in a transit EIRP at boresight of approximately 68.2 dBW, so that the maximum signal strength would be available for detection at the farthest points. The test frequency used was 29.2 GHz (the INTEX transmit license allows transmissions only from 29.1 to 30.0 GHz, the operating frequencies of the ACTS satellite).

NASA Lewis's architecture services division located and marked 15 points relative to the INTEX antenna focal point for these tests, as described later in this report. At 13 of these points (two points were omitted due to time and schedule constraints), measurements of the received field strength at horizontal and vertical polarizations were made with a pyramidal horn of 24.7 dB gain and a Lewis in-house designed and fabricated 16 X 16 element planar array antenna. Final measurement were made for three of the points using the Endgate 32 X 32 element planar array. At each measurement point, the field strength was measured in the direction toward the INTEX antenna, at $\pm$ 45°, $\pm$ 90°, and 180° from this position. The results indicated a significant variation of field strength from what would be calculated in a simple, straight-forward far-field type analysis. These variations, as will be further explained later, result from near-field effects, the reflection environment, and differences in sidelobe structure between the three antennas.

The report is presented in two separate and complete sections, Part One first dealing with the laboratory measurements and Part Two dealing with the field measurements.

Part One: LMDS/FSS LABORATORY INTERFERENCE TEST SUMMARY

Objective:
The laboratory experiment section of the LMDS test plan has the goal of establishing interference thresholds of FSS systems into LMDS systems based on C/I ratios measured at the 27.68 GHz LMDS receiver input. Additional laboratory tests involved recording SMPTE color bars along with a standard video still picture at various C/I levels ranging from no interference, to just perceptible interference, to just perceptible plus 3 dB, 6 dB, 9 dB, 12 dB, etc all at a 0 Hz frequency offset. All laboratory tests involved injecting various types of 27.68 GHz FSS modulated interference into an LMDS receiver at various frequency offsets and power levels.

Measurement Techniques:
The threshold of perceptibility measurements were performed using the SMPTE color bars only. Two non-professional viewers were used for the subjective color bar evaluation. A laboratory engineer would set up for a particular C/N at the receiver subsystem input and begin the test with no interference present. The engineer would then slowly dial in interference via RVA #3 (refer to figure 1) until the viewers perceived the onset of distortion in the color bars. The engineer would then turn off the video source and measure the FSS interference power at calibration port C. Since the video only power was already measured in the absence of any interference, a direct subtraction between the two power readings yields the C/I ratio at the threshold of perceptible distortion. The engineer now dials RVA #3 back to maximum, increments the frequency offset, and begins again to dial in more interference power until the viewers notice the distortion. This process was repeated until the interference spectrum was far enough out of the LMDS video band that more power than was available would be needed to produce any visible distortion.

The laboratory tests were conducted using different C/N ratios set at the input to the receiver subsystem. The receiver subsystem input power was calculated based on the following formulas:

$T = 290 * (10^{NF/10}-1)$ (K)
$N = 10 * \log(kTB) + 30$ dB (dBm)
$C = C/N + N$ (dBm)

NF is the noise figure of the receiver subsystem, B is the bandwidth of the 20 MHz filter prior to the demodulator, k is Boltzman's constant of 1.38×10^{-23}, and C is the required carrier video power. Thus, by first determining what C/N is desired, the receiver subsystem input power can be calculated since the noise figure and the bandwidth are both fixed. For example, if a C/N of 31 dB is desired, a video carrier power of -68.17 dBm is required at the receiver subsystem's LNA input based on a 4 dB noise figure and a 20 MHz bandwidth filter. The receiver subsystem input power required for each C/N was adjusted using RVA #2 and measured at calibration port D. Since power levels below -70 dBm can not be measured by any available power sensor, calibrated RVA #1 was first set to 0 dB and RVA #2 was adjusted to yield 30 dB greater than required power reading at port D. RVA #1 was then adjusted to 28.75 dB, which was network analyzer verified to yield exactly 30.0 dB of attenuation.

The noise figure of the receiver subsystem (see Fig. 1) was measured to be 4.0 dB by using a 30 GHz Ailtech gas discharge noise generator with an excess noise ratio (ENR) of 16.3 dB in conjunction with the HP 8970A noise figure meter.

The subjective just perceptible interference threshold was judged using SMPTE color bars in a darkened room using a single trial.

Test 1 27.5 Mbps Continuous SMSK

This satellite interference was created using a Motorola 27.5 Mbps uplink modulator designed for use with the Advanced Communications Technology Satellite (ACTS) project. This modulation scheme has a main lobe bandwidth of 1.5 times the data rate, which is 41.25 MHz. A plot of the perceptibility threshold in C/I versus frequency offset from the center of the video spectrum is shown in figure 3. The three C/N curves tend to lie close together with the C/N of 15 dB tending to be the most susceptible to the interference by having the onset of perceptibility occurring at the highest C/I.

Observations:

- Noise tends to mask the interference to some extent. At co-channel, 2 dB variability seen in C/I across C/N of 15 to 31 dB (up to 7 dB variation observed at some frequency offsets).
- In general, C/N = 15 dB provided least tolerance to interference (less headroom due to early onset of threshold).
- C/I_{tot} approximately 18-20 dB at co-channel (C/I in band would increase by about 3 dB)
- Maximum C/I_{tot} = 25 dB for C/N = 15 dB at -2 MHz offset.

Test 2 27.5 Mbps Bursted SMSK

The same Motorola modems were used for this test case as were used on Test 1. Test 2 is intended to simulate an ACTS type uplink station using a demand assignment TDMA access. The continuous spectrum is on/off modulated at two duty cycles in order to yield a total throughput data rate of T1 (1.544 Mbps) and four times T1. This was accomplished by placing a PIN diode switch after the modulator and driving the PIN diode with a 5.56% and 22.2% on time TTL signal. This corresponds to a 55.6 μsec on time and a 222.2 μsec RF on time which repeats every 1000 μsec frame. Two different methods were used to calculate the bursted interference power levels. Since only continuous averaging power meters are available, every halving of the duty cycle would produce a 3 dB loss in measured power. Bursting at a 5.56% duty cycle yields a 12.55 dB loss in power compared to the continuous case, and the 22.2% case has a 6.5 dB loss. Since these levels would require measuring very low power levels, the bursted interference power levels were measured by switching back to a 100% duty cycle and subtracting off the corresponding loss factor. Figure 4 shows the perceptibility threshold graph with the interference power calculated as an average power, meaning the loss factors have been subtracted out. This graph indicates that the single T1 burst rate (the burst rate with the shorter RF on time) is more detrimental to the video than the 4 times T1 rate.

Graphing the same curve but using a peak interference power (same as continuous power) shows that just the opposite is true. Figure 5 has the two duty cycles plotted, along with the continuous 100% duty cycle. This graph indicates that most detrimental interference is the continuous, followed by the four times T1, and the T1 being the least detrimental.

The bursted 27.5 Mbps interference produced a different distortion pattern in the color bars at low C/Is than the continuous 27.5 Mbps. As the picture quality became increasing worse, rolling horizontal lines began to form. These lines became more intense as the C/I was lowered, and the lines were wider for the four times T1 case. The continuous 27.5 Mbps interference never exhibited the horizontal lines, rather reacted to the lower C/I with more "sparks" of interference. Recordings of this interference pattern were made for future reference.

To examine the effect that frame time of the TDMA burst might have on the subjective results, a frame structure which would approximate the Teledesic TDMA burst was implemented. A 20 msec frame time with a 2 msec burst time (10% duty cycle) was tested using the method discussed above. Figure 5a overlays these results on the data shown in figure 5. These results would indicate that the just perceptible subjective effect of bursted signals is dependent on duty cycle and not on frame time.

It should be noted that the rate at which the bursted interference rolled through the wanted picture varied with the frame time. At the comparatively high frame times proposed by Teledesic (~20 msec) the interference rolled through the wanted signal more rapidly than the 1 msec frame times. In addition, the 2 msec burst rate caused a much wider band of interference in the wanted signal. At interfering levels greater than the just perceptible level, the broader more rapidly moving band of interference appeared more objectionable than the effect seen for the 1 mssec frame time cases. It should also be noted that the bandwidth of the SMSK spectrum was 41.25 MHz compared to 27 MHz for a QPSK modulated signal as proposed by Teledesic. The C/I in band for a 27 MHz QPSK spectrum would be approximately 2 dB greater [10log(41.25/27)] than the results shown. The effect of SMSK spectral shaping compared to the abrupt transitions of a QPSK signal need further assessment.

Test 3 T1 QPSK Interference

This interference was generated using a ComStream CM421 digital multirate modem.
Three different C/Ns were tested for the perceptibility threshold as indicated in figure 7. Figure 6 is the same as figure 7 except only the C/N of 31 is plotted in order to easily show the frequency offset influence.

The interference characteristic of the narrow T1 signal displayed interference in different locations of the SMPTE color bars. For example, at a 0 Hz offset the distortion would appear mostly in the red color bar, but as the offset varied in 1 MHz increments the distortion would be most visible in the color bar directly adjacent to the red. Further increases in the offset would then move the distortion to the next adjacent color bar.

Observations:

- Significant variation in C/I with frequency offset - caused by interference moving through different spectral bands of the color bar signal (effect less pronounced on test slide material).
- Generally, C/N = 15 dB less tolerant to interference.
- At co-channel, C/I = 24-28 dB required for just perceptibility

Test 4 Three T1 QPSK Interferers

This interference test involved placing three identical QPSK T1 sources spaced at 2.5 MHz center to

center. The offsets from the video center are measured from the middle T1 spectrum. Figure 8 shows the graph for both a C/N of 15 dB and a C/N of 31 dB.

The interference in the color bars for the three T1 case seems to affect select portions of the screen similar to the single T1 signal, but the three T1 case affects multiple areas of the screen.

Observations:

- Significant variation in C/I with frequency offset - caused by interference moving through different spectral bands of the color bar signal (effect less pronounced on test slide material).
- Generally, C/N = 15 dB less tolerant to interference.
- C/I's of 28 dB required for some frequency offsets when C/N = 15 dB. (Spectral sensitivity).

Additional Tests

A comparison between the C/N and the S/N as measured by a Tektronix VM 700A Video Measurement Test set is shown in figure 2. Two different NTC7 S/Ns were plotted, and the S/N measured by the Tektronix was the limiting factor in going to lower C/Ns. Any decrease in C/N beyond 12 dB produced to low of a S/N for the Tektronix to maintain lock.

Part Two: LMDS/FSS Field Measurements

INTRODUCTION

The interest in the field measurements expressed by members of the IWG stems from the lack of information available regarding the behavior of fields from an FSS uplink at 28 GHz in terms of reflections, multipath, and near-field effects, combined with uncertainties in the transmit and receive antenna sidelobe structures. The NASA Lewis tests suggested in the draft test plan were intended to address some of these important points. Originally two tests were suggested; one test would measure received power at several points relative to a transmitting FSS uplink antenna, a second test would measure the general reflection environment due to buildings and structures in the area of the FSS uplink antenna. Due to severe time constraints, these two types of tests were combined into one, as described below.

The results of the field measurements are expressed in terms of received power for the horizontal and vertical receive antenna polarizations, for several directions, for each receive antenna, and for several measurement directions at each point as described below. The result is a large number of measurements, 324 in all, describing the field environment in the vicinity of the transmitting antenna.

The following sections describe the location of the measurement points and the general methodology of the measurements, followed by the results and preliminary comments and observations. It should be emphasized that the entire test setup and execution took place within a nine day period, and was additionally constrained by the ACTS experiment schedule, the availability of measurement equipment, the availability of the Endgate antenna, the ability to close sections of the Lewis campus to vehicular traffic, and the time requirement to locate and mark the measurement points. These factors

combined to limit the number of measurements to be made, making the analysis of the resulting data somewhat more difficult. To fully characterize the environment in the vicinity of the transmitting antenna would require a far greater number of measurement points. The results obtained, however, give considerable insight into the types of problems that may be encountered when working with FSS uplinks at Ka-band frequencies.

GENERAL TEST PARAMETERS

The field tests were conducted at the NASA Lewis Research Center in Cleveland, Ohio. The appropriate satellite uplink used is known as the INTEX Ka-band Experiment Ground Terminal. The INTEX terminal uses a 2.44 meter cassegrain-fed parabolic reflector antenna, and was designed to operate in the 29.1-30.0 GHz uplink band of NASA's Advanced Communications Technology Satellite (ACTS). ACTS is currently the only Ka-band communications satellite in existence in the Western Hemisphere. The INTEX terminal is the appropriate terminal for use in these tests, since it has a 40 Watt transmitter, is located on the ground, rather than on a roof top, and has a reasonable amount of working space available around it.

For these tests, the INTEX antenna transmitted a CW tone at 29.2 GHz, at the maximum power level of 40 Watts. Considering transmit feed losses and antenna gain, the transmit EIRP on the boresight axis is approximately 68.2 dBW. This maximum transmit level is adequate for closing the ACTS link at 220 Mbps. It was chosen for this test in order to provide the maximum field intensity so that reliable measurements could be obtained at the farthest measurement locations. A CW signal was used for this test, rather than a modulated signal, so that it could be most easily identified and measured. The antenna pattern model for this antenna is shown in Fig. 13b. The INTEX antenna transmits in the horizontal polarization; the polarization tilt due to the longitude difference between the ACTS satellite and INTEX is approximately 18°.

Three receive antennas were used for these tests. The first was a 16 X 16 element planar array designed and fabricated in-house at Lewis. The array has approximately 23 dB of gain, and the measured antenna pattern is as shown in Figs. 12a and 12b. The second was a standard pyramidal horn, with 24.7 dB gain. The measured pattern for this horn is shown in Fig. 13a. The third receive antenna was a 32 X 32 element planar array developed by Endgate Corporation and provided on loan to NASA Lewis. The measured antenna pattern for this array (measured at NASA Lewis) is shown in Figs. 13c and 13d; the gain measured by NASA Lewis (including feed and connector losses) is approximately 22 dB. The horn antenna and the Lewis Array were used at all the of 13 locations. The Endgate array, due to time constraints and some difficulties encountered in the antenna pattern measurements, was used at three locations.

LOCATION OF MEASUREMENT POINTS

The measurement point locations were chosen to give a representative selection of points within the vicinity of the transmission. Figure 9 shows the measurement locations relative to the INTEX antenna. Locations were chosen along four axes radiating from the INTEX focal point. The 0° axis corresponds to the INTEX antenna boresight. The other axes were 30°, 45°, and 90° from the 0°

line. Several distances were chosen for these measurement locations: 200 feet, 400 feet, 500 feet, 1000 feet, and 1500 feet. The major constraint in determining these locations was the physical and geographic environment at the Lewis campus. Specifically, buildings and structures, as well as two man-made ponds and a ravine, had to be considered in choosing the locations.

In figure 11, the measurement locations are superimposed on a map of the Lewis Research Center. This map indicates the various major obstructions in the line of sight from the measurement locations to the INTEX antenna. Ultimately, measurements were made at 13 of the 15 points. Two points were omitted due to time constraints and difficult terrain (including poison ivy).

TEST SETUP

The receiver used for these tests was a Hewlett-Packard 8560E 30 GHz portable spectrum analyzer. The spectrum analyzer was connected to the receiving antenna through a 5 foot coaxial cable . The power loss through the cable at 29.2 GHz was measured to be approximately 3.5 dB. Including connector losses at the cable/antenna interface, approximately 4 dB should be added to the spectrum analyzer measurement to accurately assess the actual received power. A plotter was used to record the spectrum analyzer results for the measurements made in the direction of the INTEX antenna only (time constraints made plotting of all measurements impractical). Examples of these plots are shown in Figures 14-18.

TEST PROCEDURE

The array antennas were mounted on a calibrated tripod which could be easily rotated in elevation and azimuth. The horn antenna did not have a suitable tripod mount available. At each measurement location, six pairs of measurements were made for each antenna. The first measurement was made with the receive antenna pointed directly at the INTEX antenna. This is referred to as the 0° direction. The receive antenna was then rotated in azimuth by 45° clockwise (referred to as 45° E) and counterclockwise (referred to as 45°W), then by 90° clockwise (referred to as 90° E) and counterclockwise (referred to as 90° W), and finally by 180° (referred to as 180°). For each of these six directions, a separate measurement was made with the receive antenna aligned in the vertical polarization and the horizontal polarization.

For each measurement, the array antennas could be rotated by using the calibrated tripod for rotation. For the horn antenna measurements, the array antenna was first aligned in the appropriate direction, and the horn was manually aligned using the array as a guide. This results in a slightly higher potential pointing error for the horn measurements.

At each measurement direction, the azimuth of the receive antenna was fixed. The elevation was varied from 0° to 30° and the maximum value of received signal was recorded by the spectrum analyzer. The reason for this variation was that in some of the measurements (those not pointed directly at INTEX or those without a direct line of sight to INTEX) the elevation angle resulting in the maximum received power varied. Since small variations occurred even at line of sight locations, the only practical way to record the maximum received powers was to vary the elevation in this way. The alternative; to make measurements at several elevation angles, would not be practical within the

available time.

Where a line of sight was available, the maximum power was achieved at elevation angles of approximately 2° to 6° for the Lewis array and horn, and approximately 0° to 3° for the Endgate array. Where the line of sight was not available, the major source of received power was reflections, which were occasionally found to occur at higher elevation angles. In all cases, no received power maximum occurred at an elevation angle greater than 20°.

TEST RESULTS

For each of the 324 measurements made, a spectrum analyzer display was obtained in which the INTEX signal at 29.2 GHz was identified and the power level of the peak signal measured. These displays were plotted for the cases where the receive antenna was pointing directly at INTEX. For the other cases, the power level measured by the spectrum analyzer was recorded by hand.

Examples of the spectrum analyzer displays are shown in Figs. 14-18. Shown are the measurements for the horn, the Lewis array, and the Endgate array at a distance of 200 feet on the INTEX boresight, with the antennas horizontally oriented, and for the horn and Lewis array at 1500 feet on the INTEX boresight, with the antennas horizontally oriented, respectively. For 12 of the 13 points measured, a clearly discernible signal could be identified and measured. For point 13, no signal could be identified above the noise floor.

It is important to state the repeatability of the measurements made. For a number of trials, measurements were repeated, both with and without movements of the receive antenna. In these trials, the repeatability of the measurements was approximately ± 1 dB.

Tables 1 through 4 list all of the measured results. Table 1 gives the results for measurement locations 1 through 5, all of which are located along the INTEX boresight, at distances of 200, 400, 500, 1000, and 1500 feet, resp. Each row gives the measured vertical polarization measurement (V) and horizontal polarization measurement (H) for the Lewis array, the horn, and the Endgate array (measured at points 1-3 only), for each of the measurement directions. The 0° direction has the receiving antenna pointing directly toward the INTEX antenna, the 180° direction has the receiving antenna pointing directly away from the INTEX antenna, and the other four measurements are points in between these two extremes.

Table 2 gives the results for locations 6, 7, and 8, all located 30° from the INTEX boresight at distances of 200, 400, and 500 feet, respectively. Measurement results are given similarly to Table 1 for the Lewis array and the horn.

Table 3 gives the results for locations 10, 11, 12, and 13, all located 45° from the INTEX boresight at distances of 200, 400, 500, and 1000 feet, respectively. Measurement results are given similarly to Table 1 for the Lewis array and the horn. Again, note that no signal was detected above the noise floor at location 13.

Table 4 gives the results for location 14, located 90° from the INTEX boresight at distances of 200 feet. Measurement results are given similarly to Table 1 for the Lewis array and the horn.

It should be noted that measurement locations 1, 2, 3, 4, 6, 7, and 10 have a clear line of sight to the INTEX antenna. Locations 5, 11, and 14 experience partial blockage, and locations 8, 12, and 13 experience complete blockage.

COMMENTS AND OBSERVATIONS ON TEST RESULTS

An important factor to note is that all of the measurement points are in the near field of the antenna. Table 5 indicates the boundary of the far-field region for various sizes of antennas. The field strength in the near field is not inversely proportional to the distance squared, as would be true for the far-field case. Figure 19 shows the power density distribution in the near field.

Table 1 shows that for the boresight case, while looking directly at the INTEX antenna, one can observe that the horizontal component actually increases in strength when moving from 200 feet to 400 and 500 feet; this result occurred for all three receive antennas. This effect is attributed to the near-field distribution.

For most cases, the horizontal component is stronger than the vertical component, due to the fact that the INTEX antenna transmits a horizontal polarization. The are some cases where the opposite is true, such as location 7, due to depolarization occurring in the INTEX antenna sidelobes, as well as the results of reflections.

Table 5 - Far-field boundary as a function of antenna size

Far field as a Function of Antenna Size at 28.5 GHz			
Antenna Size, ft	Antenna Size, m	Far-field, ft	Far-field, m
0.33	0.10	6.24	1.90
0.66	0.20	24.95	7.60
0.98	0.30	56.14	17.11
1.31	0.40	99.80	30.42
1.64	0.50	155.93	47.53
1.97	0.60	224.54	68.44
2.62	0.80	399.19	121.67
3.28	1.00	623.73	190.11
3.94	1.20	898.18	273.76
4.92	1.50	1403.40	427.76
5.91	1.80	2020.90	615.97
6.56	2.00	2494.94	760.46
7.22	2.20	3018.87	920.15

8.01	2.44	3713.46	1131.86
8.53	2.60	4216.44	1285.17
9.19	2.80	4890.07	1490.49
9.84	3.00	5613.60	1711.03
11.48	3.50	7640.74	2328.90
13.12	4.00	9979.74	3041.83
14.76	4.50	12630.61	3849.81
15.42	4.70	13778.28	4199.62
16.40	5.00	15593.35	4752.85

Insight into the reflection environment in the vicinity of the INTEX antenna can be obtained by observing the differences between the 0° and 180° measurements. The differences range from 30 dB (e.g. horn at location 7, horizontal polarization) to 0 dB (e.g. horn at location 8, horizontal polarization.)

In assessing the results measured in directions other than 0° it is important to note the differences in sidelobe structure between the antennas. In particular, the element spacing for the Lewis array leads to some large grating lobes, which result in a larger reception of signals impinging on the antenna 90° from boresight.

Finally, in assessing the wide and unexpected variability in received signal strengths, it is important to note the relationship of buildings and other structures. During the measurements, it was often very easy to predict when an unusually high received power would be measured by observing buildings and structures which were positioned to provide good reflective paths from INTEX to the receive antenna. This can be analyzed with the help of Figure 11. The best example can be found by observing the difference in results between locations 12 and 13. Both points suffer from complete blockage, but location 12 has a reflective path by which signals can enter the area, while location 13 does not.

In Table 6, a simple analysis is presented to compare the expected results using a far-field analysis with the measured results. Note that in some cases, the measured power is higher than the expected result.

Table 6 - Analysis of Expected "Far-field" Results, compared to measured results, for 0° measurements (horizontal and vertical powers have been added)

Measurement Point No.	Angle relative to INTEX boresight, deg	Distance from INTEX antenna, feet	Transmit EIRP, dBm	Free space loss, dB	Expected Receive Power, Array, dBm	Actual Receive Power, Array, dBm [1]	Expected Receive Power, Horn, dBm	Actual Receive Power, Horn, dBm [1]
1	0	200	35.5	97.5	-40.0	-49.9	-37.3	-46.9
2	0	400	35.5	103.5	-46.0	-43.5	-43.3	-35.8
3	0	500	35.5	105.4	-47.9	-46.5	-45.2	-43.0
4	0	1000	35.5	111.4	-53.9	-59.3	-51.2	-50.6
5 *	0	1500	35.5	115.0	-57.5	-77.0	-55.2	-70.8
6	30	200	33.0	97.5	-42.5	-40.7	-39.8	-39.2
7	30	400	33.0	103.5	-48.5	-56.1	-46.8	-40.7
8 **	30	550	33.0	106.2	-51.2	-71.3	-48.5	-65.4
10	45	200	33.0	97.5	-42.5	-44.1	-39.8	-39.6
11 *	45	400	33.0	103.5	-48.5	-62.9	-45.8	-56.7
12 **	45	500	33.0	105.4	-50.4	-79.9	-47.7	-76.2
13 **	45	1000	33.0	111.4	-56.4	<-84.0	-53.7	<-84.0
14 *	90	200	37.0	97.5	-38.5	-54.6	-35.8	-49.0

[1] 4 dB has been added to compensate for cable and connector loss

* Points experiencing partial blockage from line of sight

** Points experiencing total blockage from line of sight

ASC LABORATORY SIMULATION OF FSS/LMDS INTERFERENCE
NASA Lewis Research Center

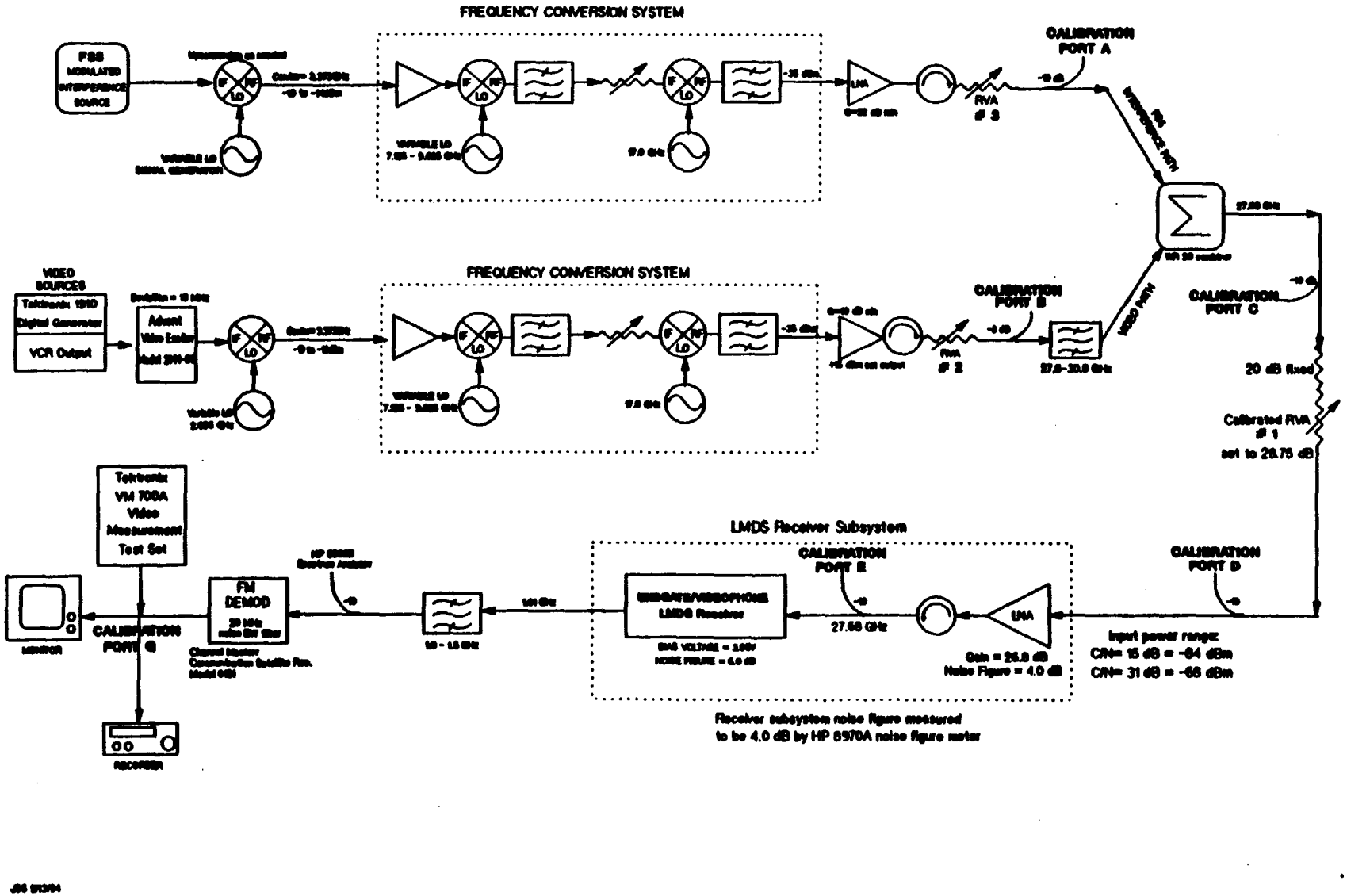

Figure 1 Block diagram of the test setup for the laboratory simulation of interference of FSS uplinks into an LMDS receiver

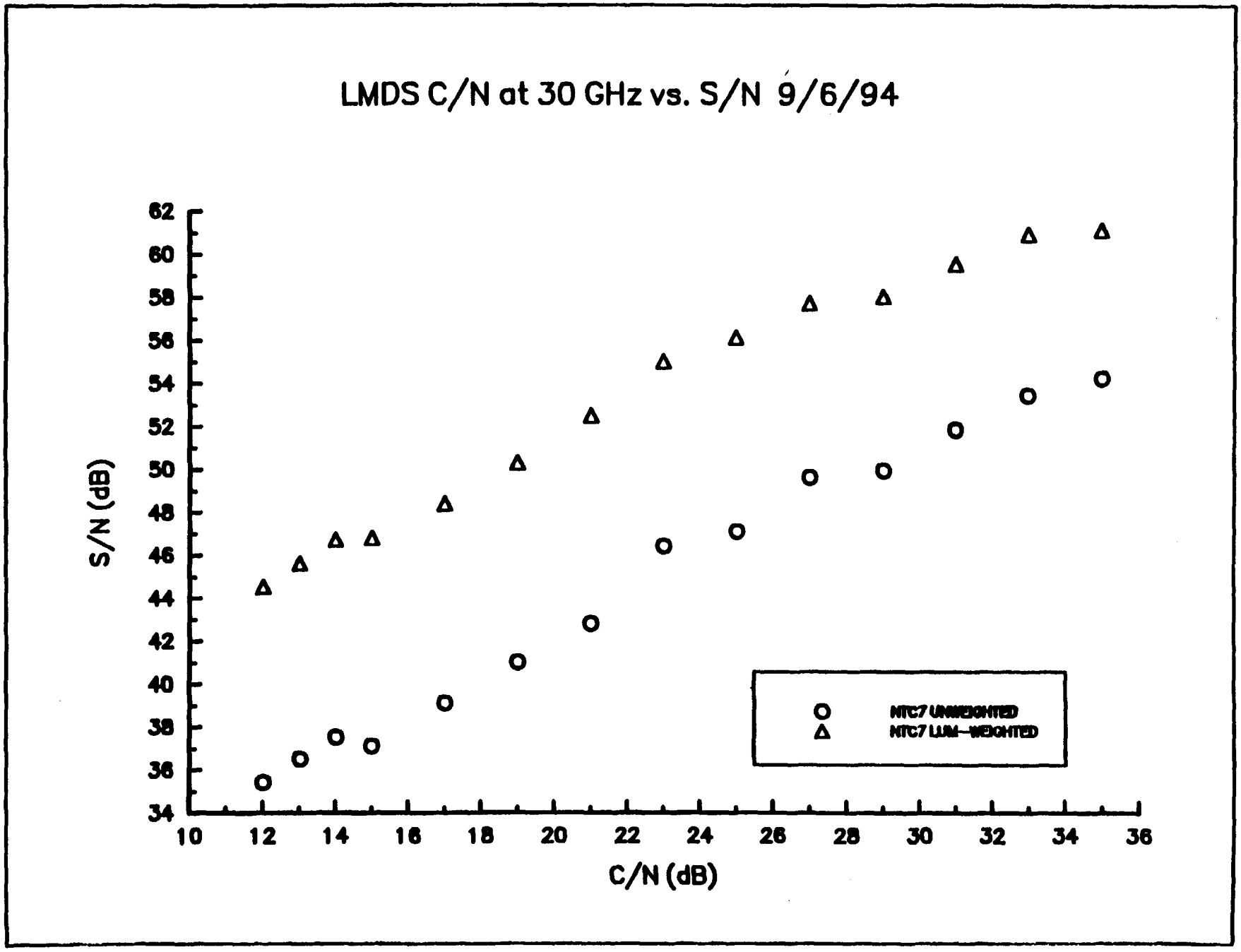

Figure 2 Output video signal-to-noise ratio as a function of input carrier-to-noise ratio for the simulated LMDS receiver

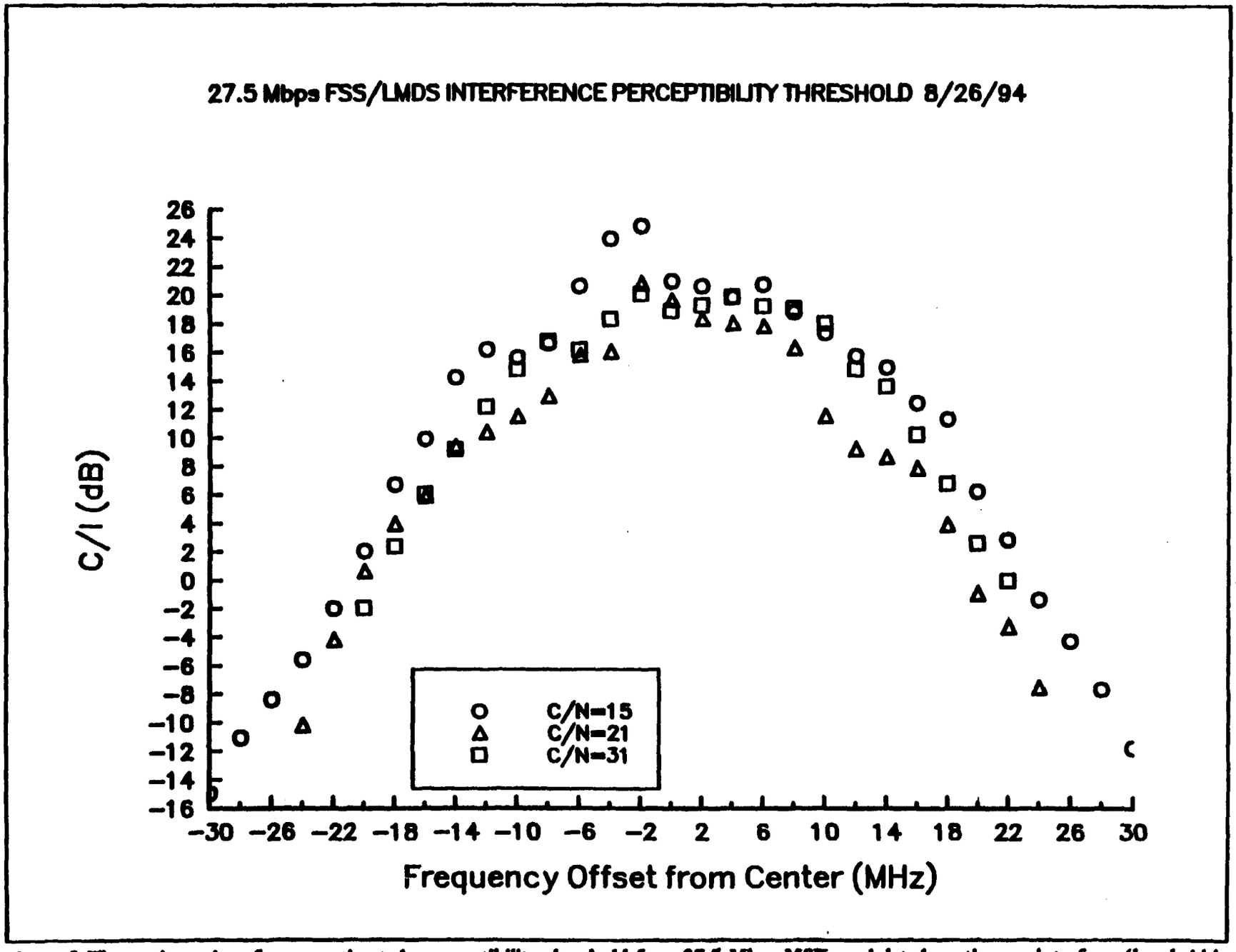

Figure 3 The carrier-to-interference ratio at the perceptibility threshold for a 27.5 Mbps MSK-modulated continuous interferer (bandwidth of 41.5 MHz) as a function of interferer center frequency offset relative to the video channel center frequency, for three input carrier-to-noise ratios

FIGURE 4 - Bursted 27.5 Mbps FSS/LMDS INTERFERENCE PERCEPTIBILITY THRESHOLD C/N=31 dB

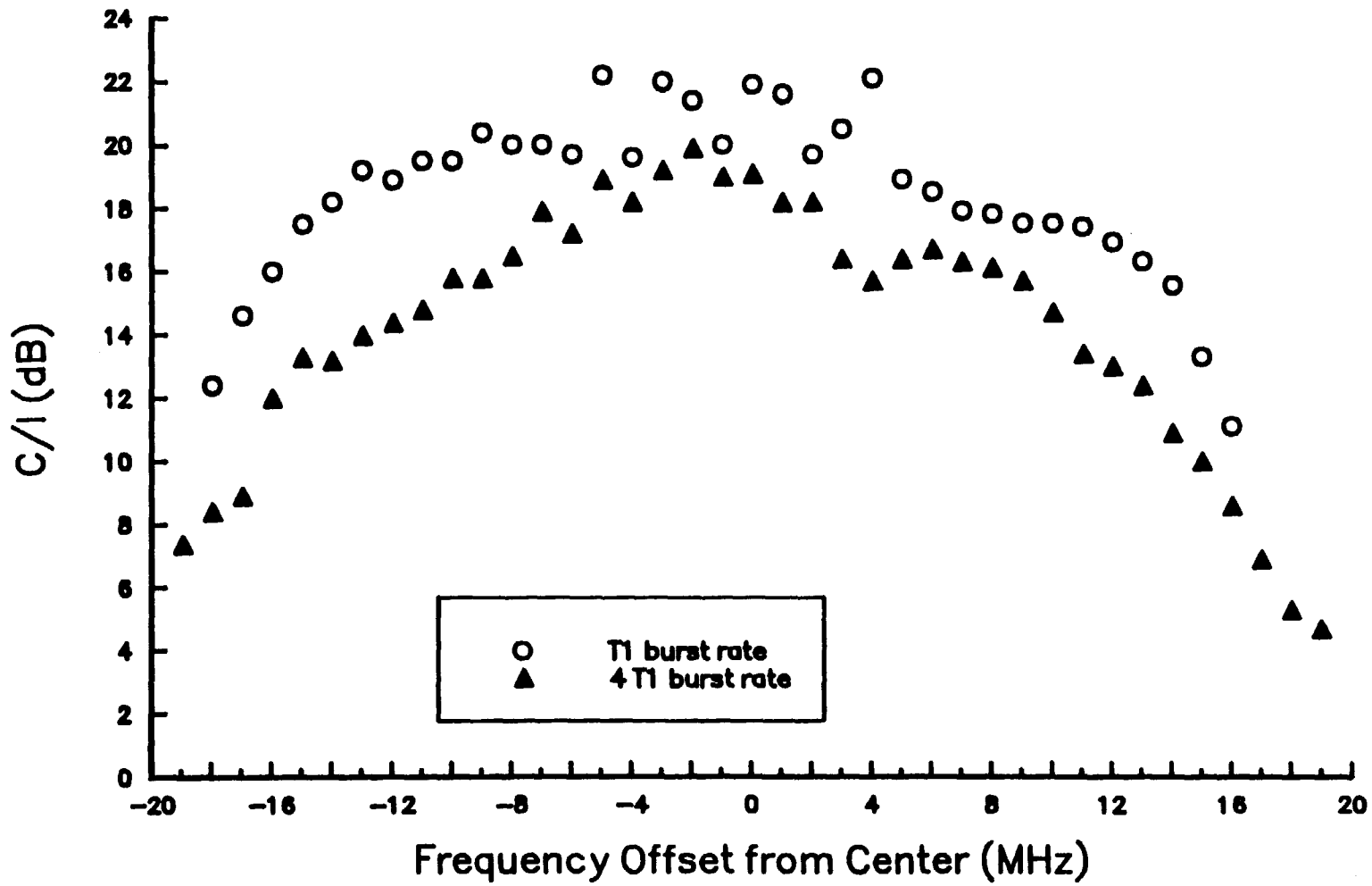

Fig 4

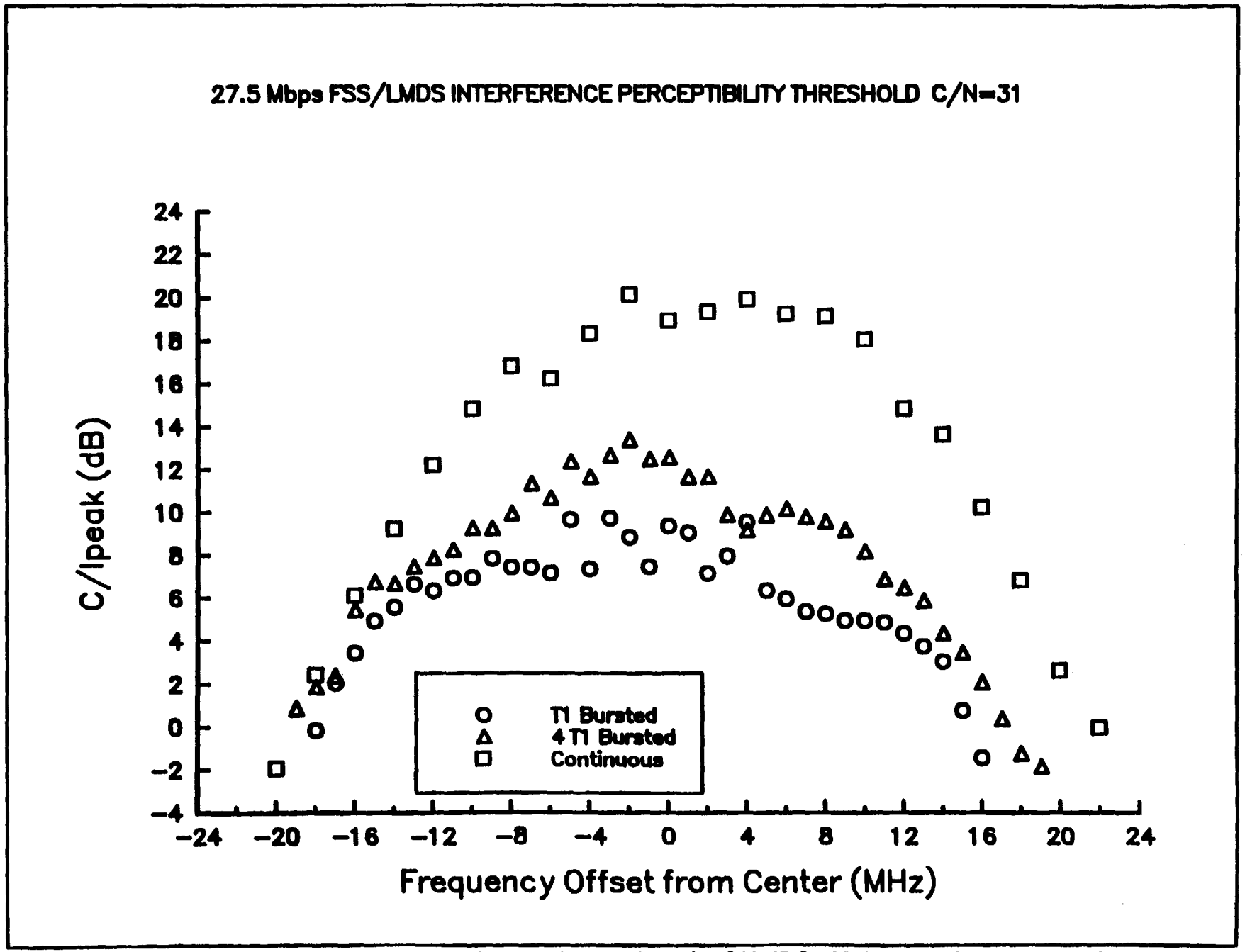

Figure 5 Comparison of perceptibility threshold results at carrier-to-noise ratio of 31 dB for 27.5 Mbps MSK continuous, 5.6% burst duty cycle (T1 rate), and 22.5% burst duty cycle (4 X T1 rate).

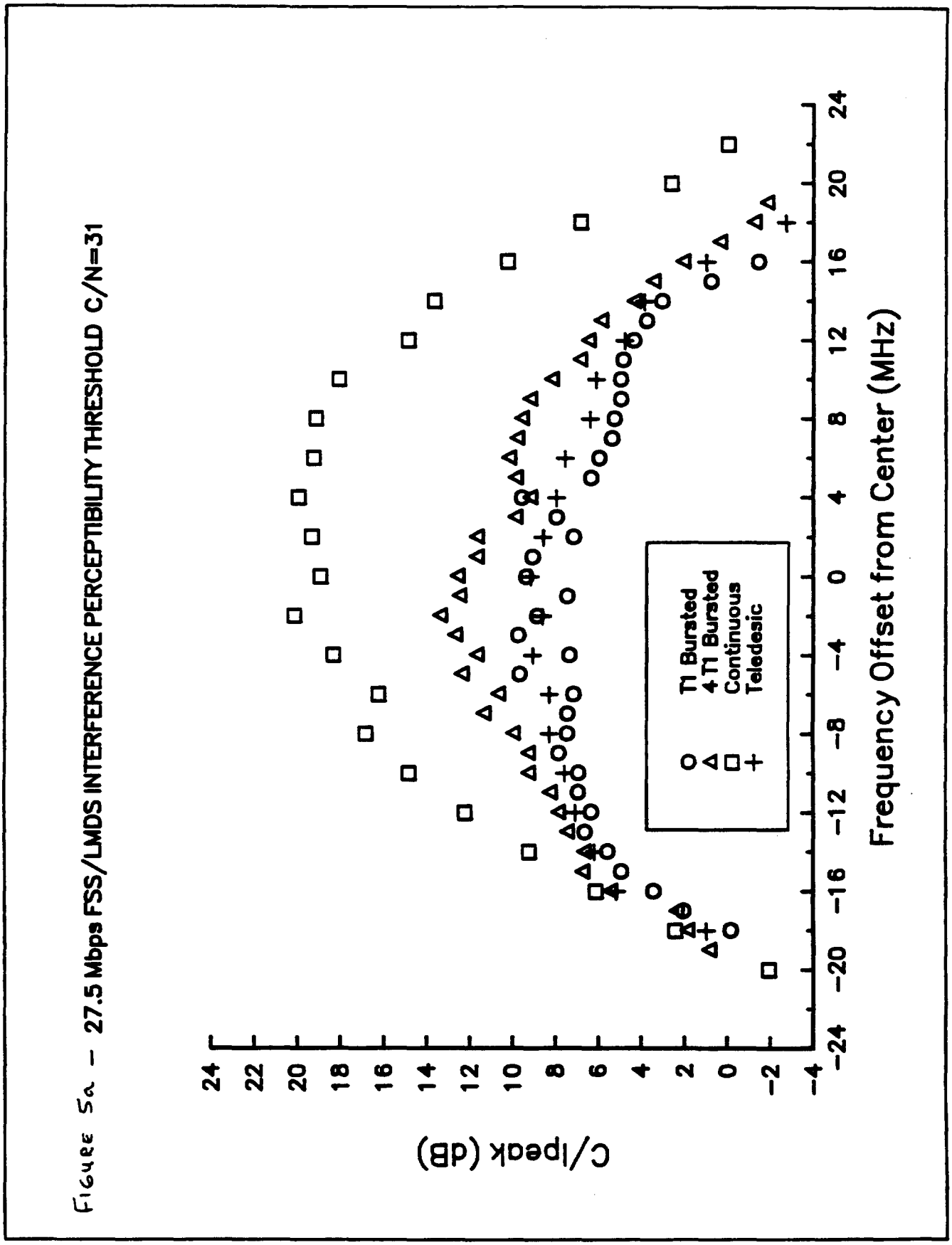
27.5 Mbps FSS/LMDS INTERFERENCE PERCEPTIBILITY THRESHOLD C/N=31
C/Ipeak (dB)
Frequency Offset from Center (MHz)
T1 Bursted
4 T1 Bursted
Continuous
Teledesic

Figure 5a –

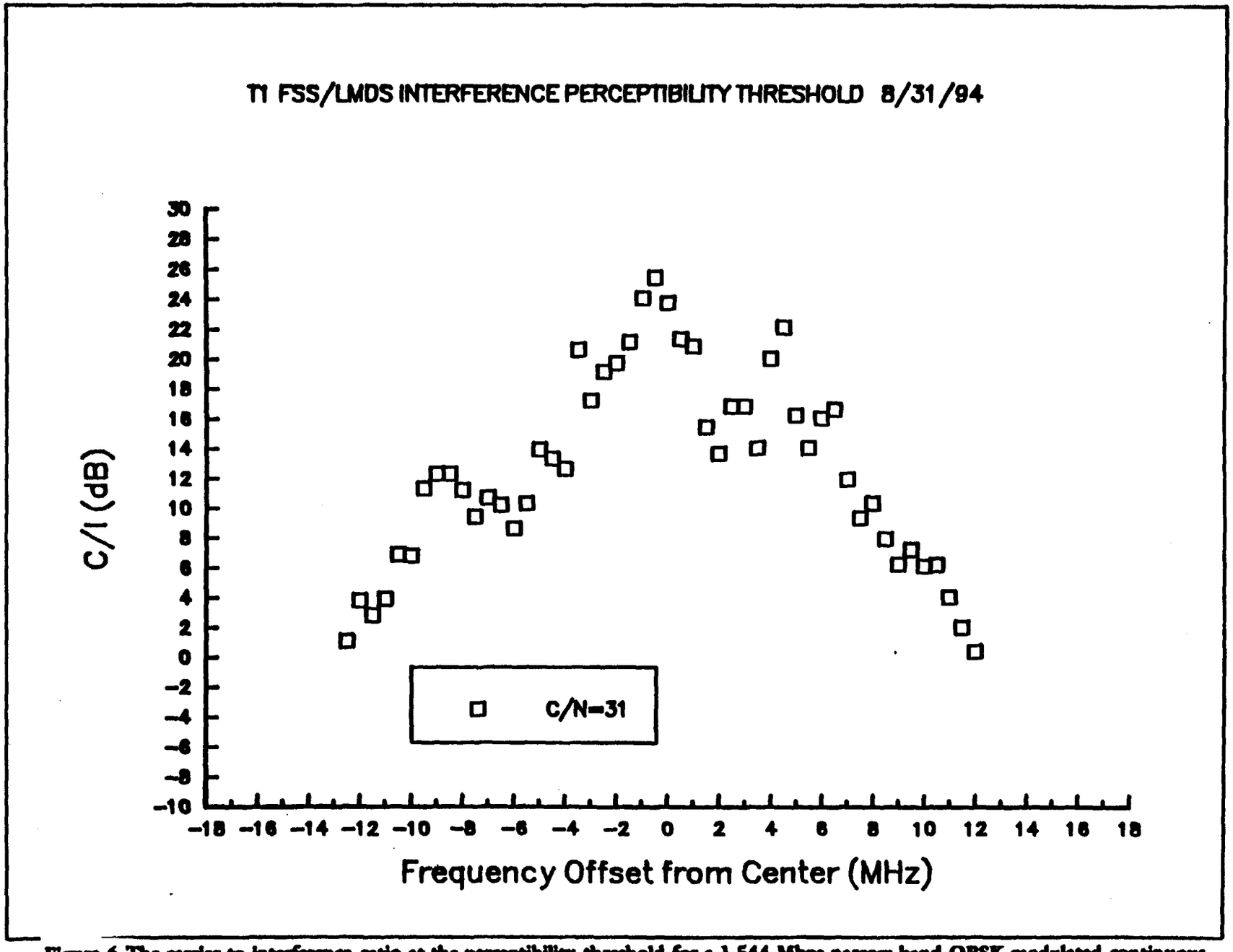

Figure 6 The carrier-to-interference ratio at the perceptibility threshold for a 1.544 Mbps narrow-band QPSK-modulated continuous interferer (bandwidth of 1.544 MHz) as a function of interferer center frequency offset relative to the video channel center frequency, at an input carrier-to-noise ratio of 31 dB

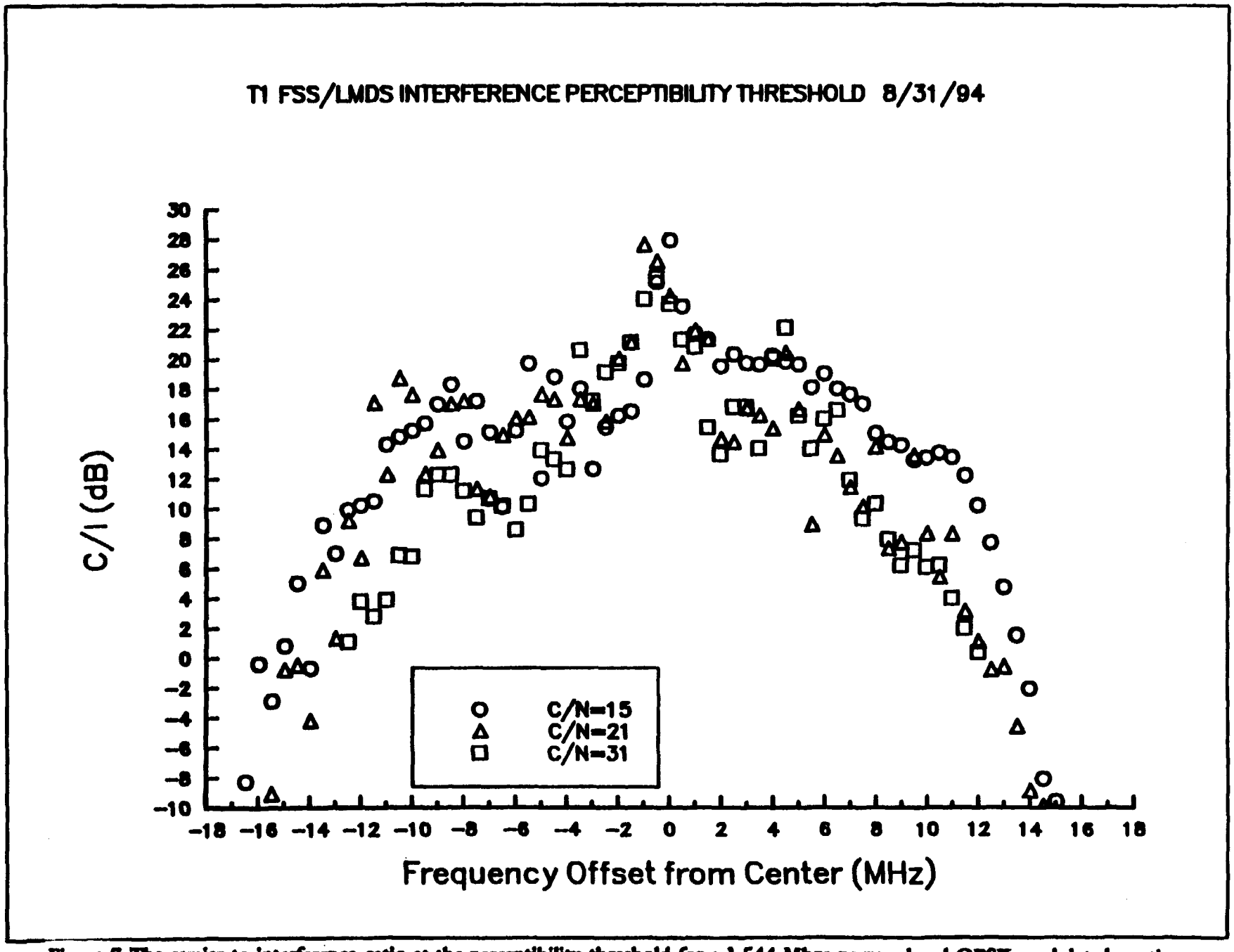

Figure 7 The carrier-to-interference ratio at the perceptibility threshold for a 1.544 Mbps narrow-band QPSK-modulated continuous interferer (bandwidth of 1.544 MHz) as a function of interferer center frequency offset relative to the video channel center frequency, for three input carrier-to-noise ratios

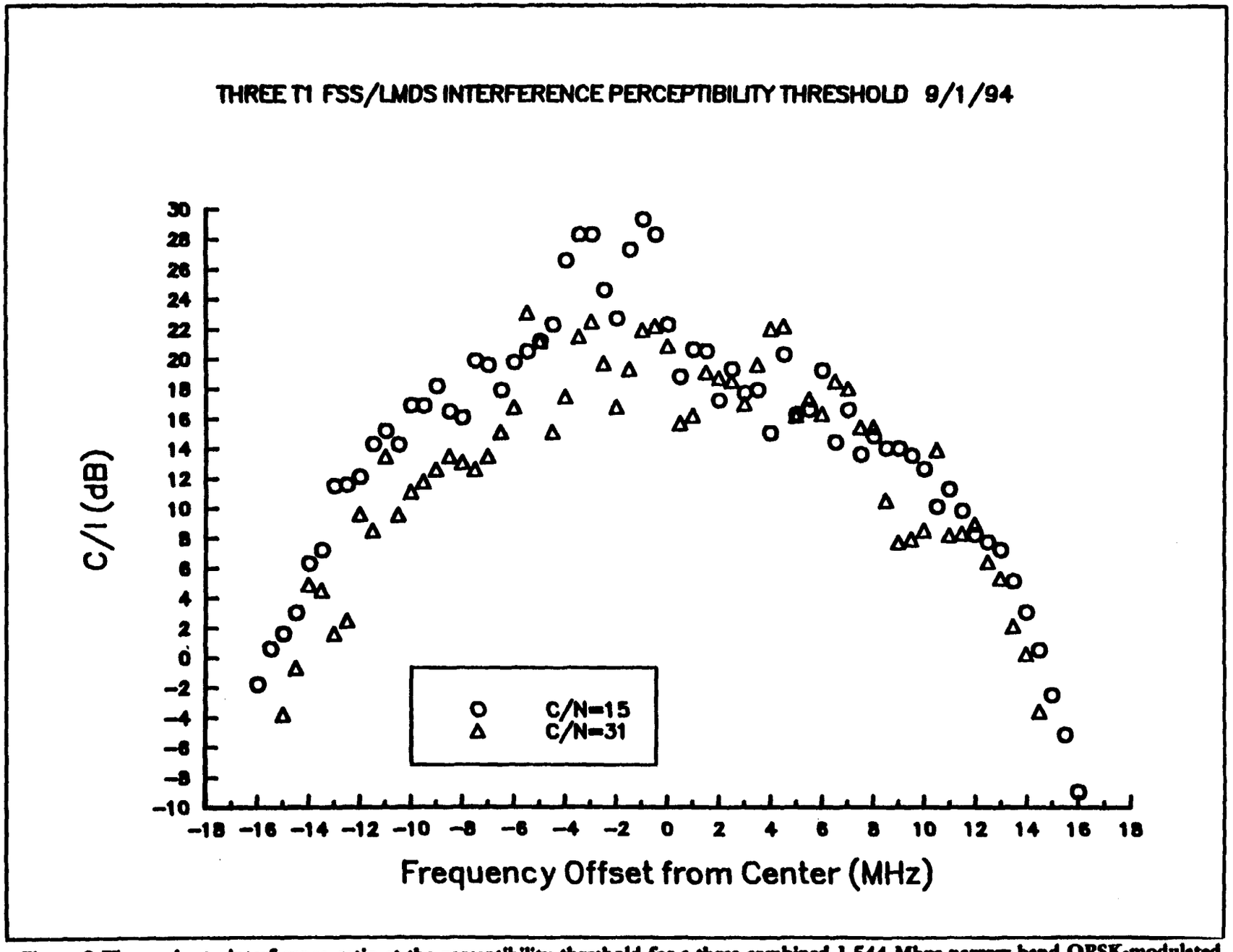

Figure 8 The carrier-to-interference ratio at the perceptibility threshold for a three combined 1.544 Mbps narrow-band QPSK-modulated continuous interferers (bandwidth of 1.544 MHz, center frequencies separated by 2 MHz) as a function of interferer center frequency offset relative to the video channel center frequency, for two input carrier-to-noise ratios

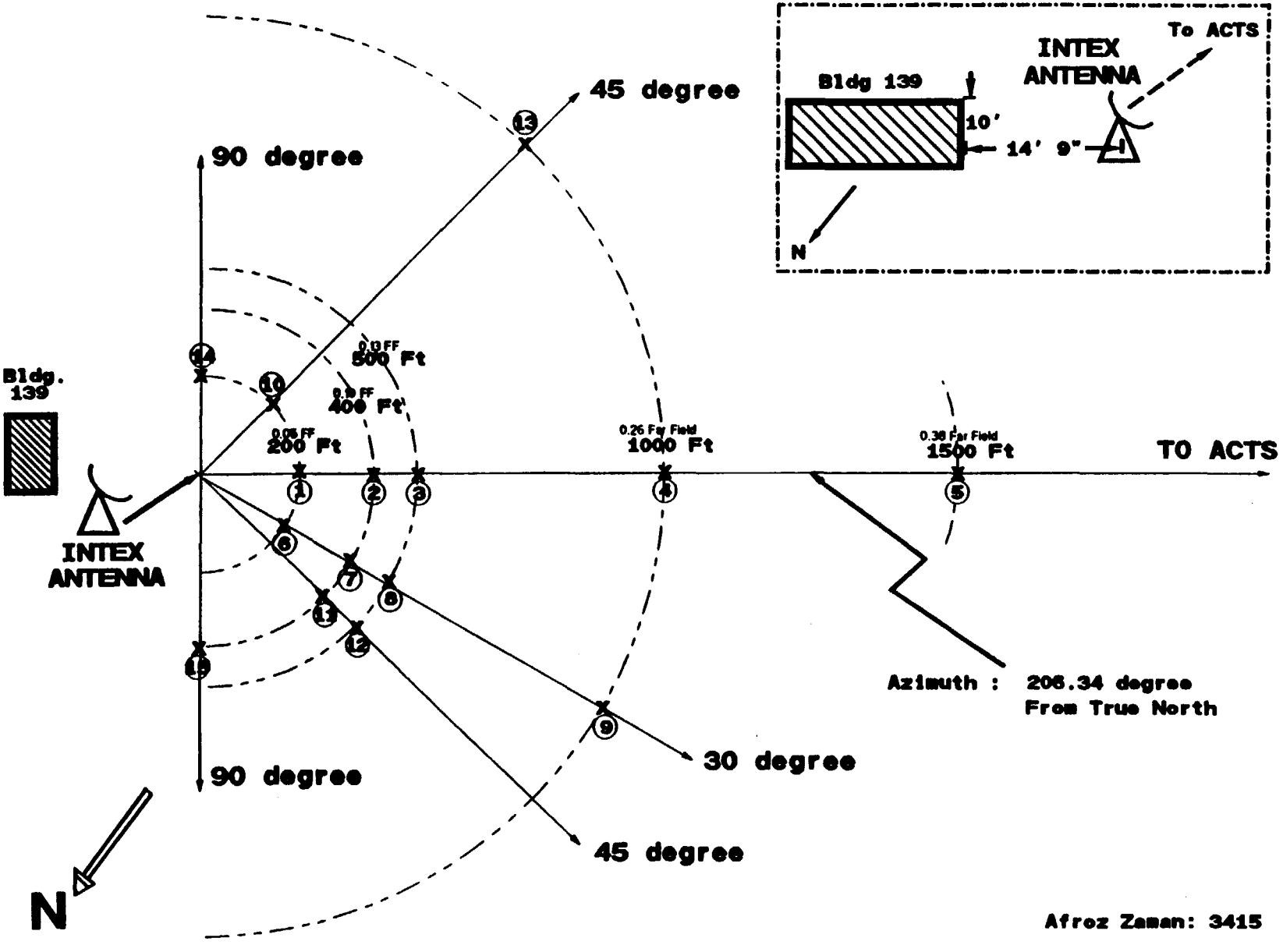

Figure 9 Positions of field measurement points relative to INTEX antenna boresight

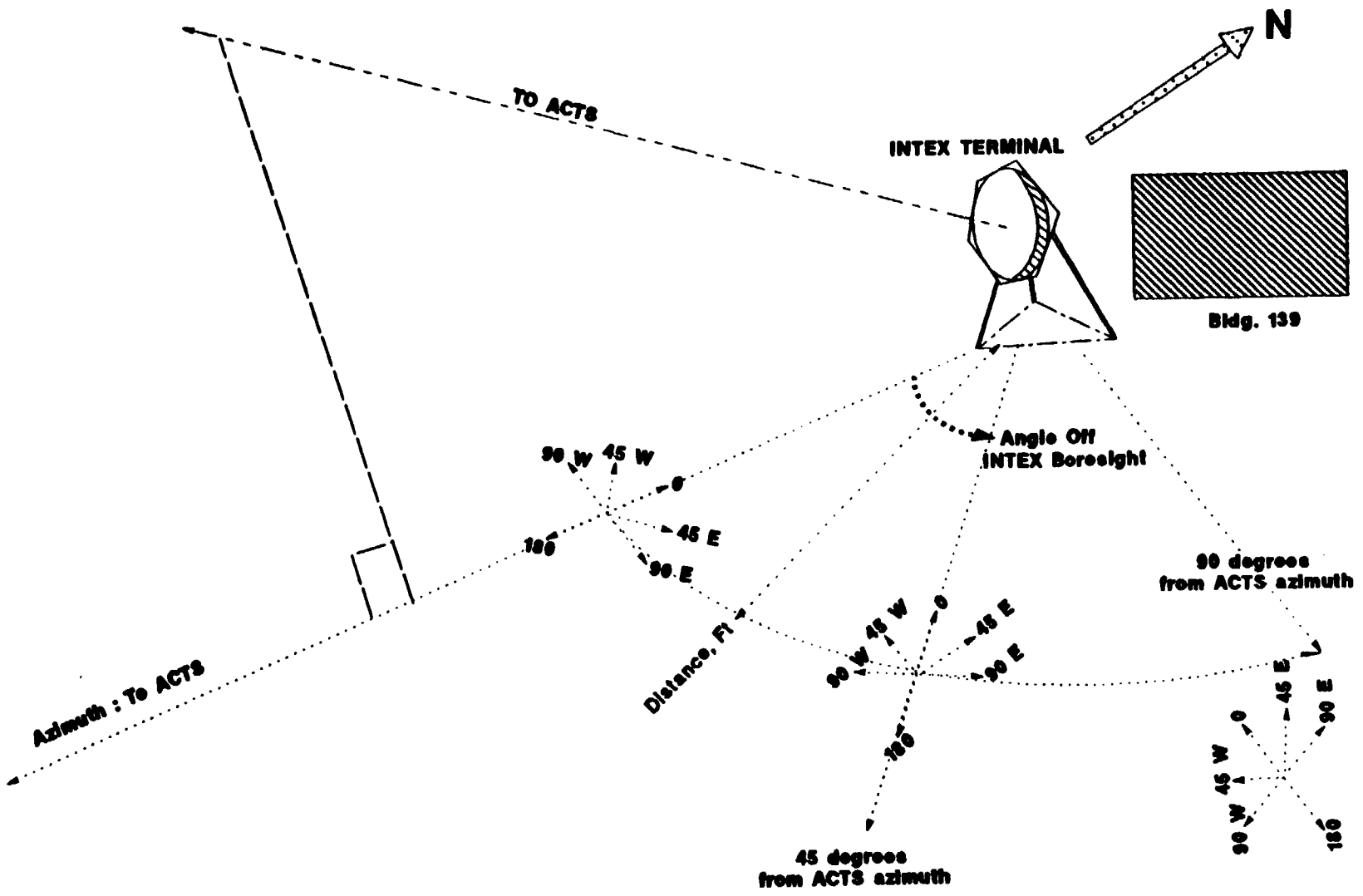

Figure 10 Description of receive antenna pointing directions used in field measurements

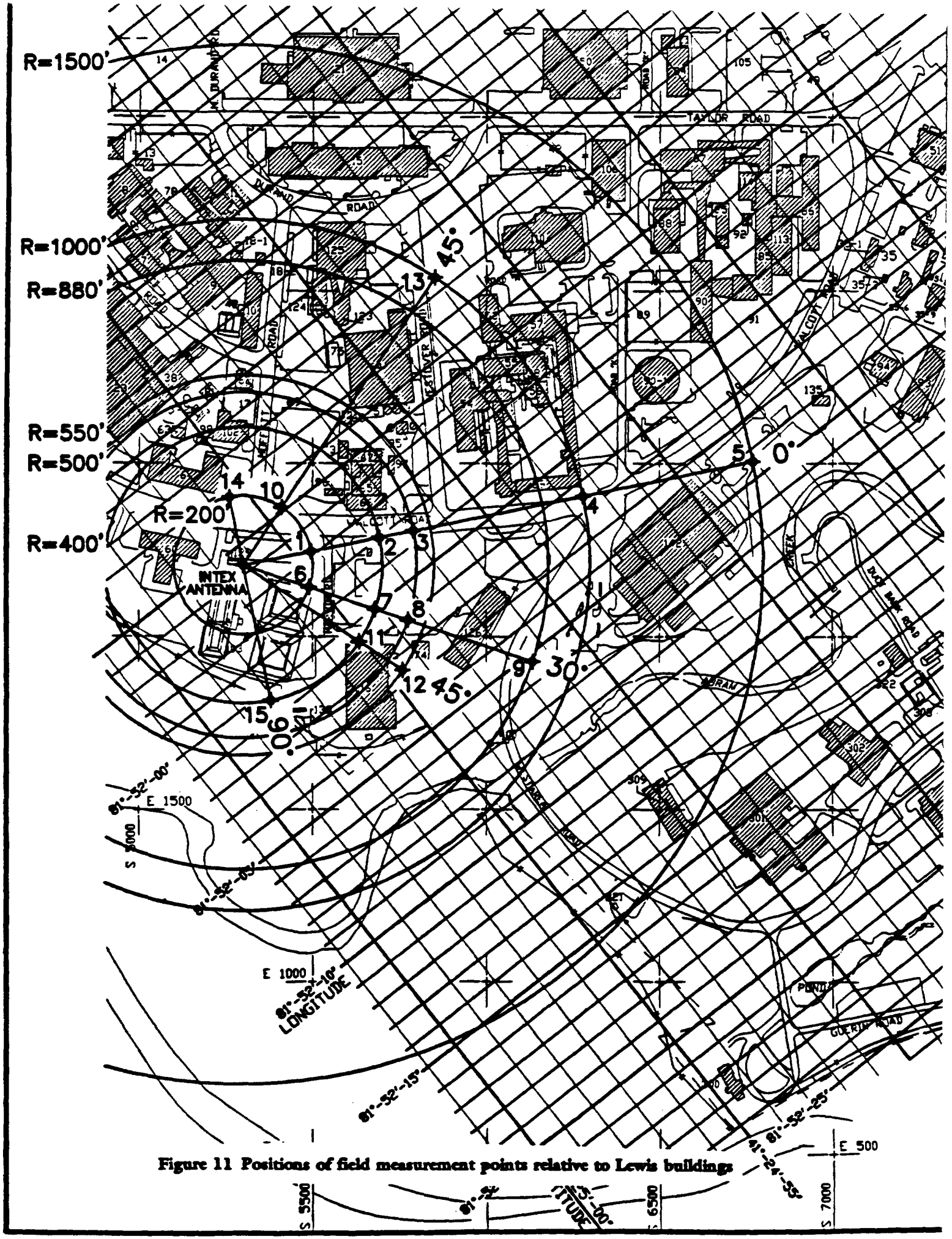

Figure 11 Positions of field measurement points relative to Lewis buildings

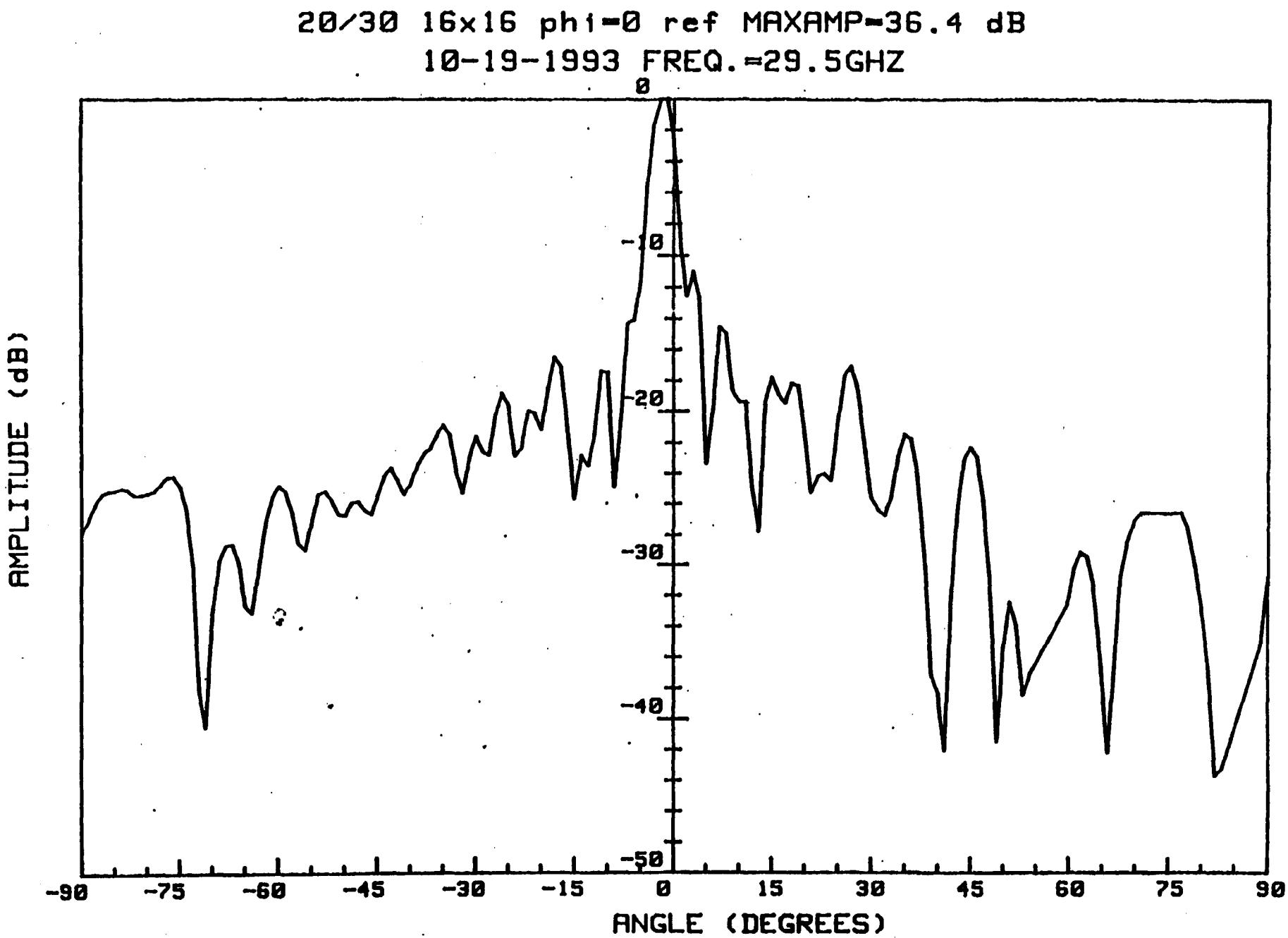

Figure 12a **E-plane antenna pattern for Lewis array antenna**

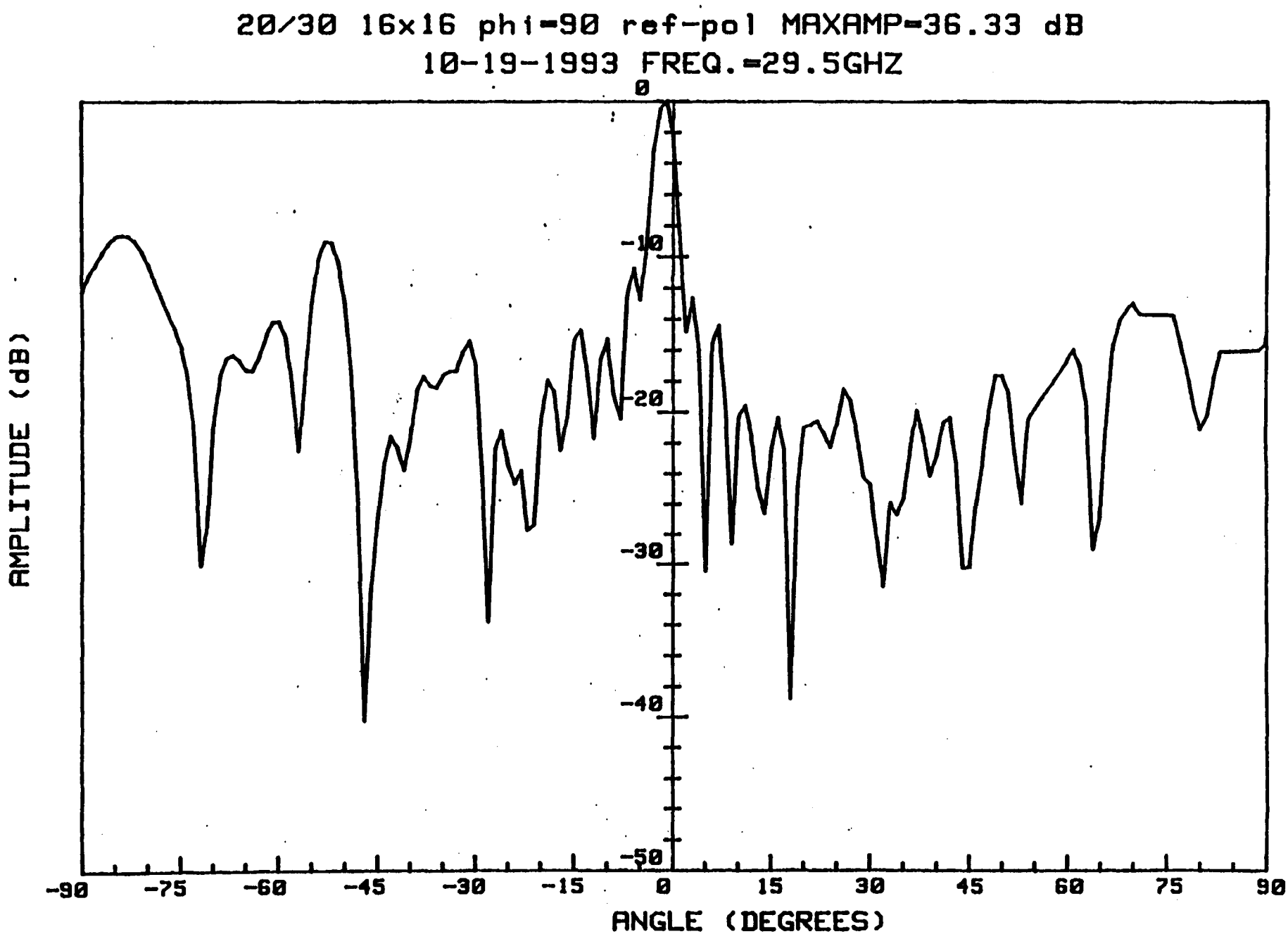

Figure 12b H-plane antenna pattern for Lewis array antenna